2004

Experimental and Numerical Study of the Flow and Heat Transfer in Plate Heat Exchanger Channels

Damir Dovic
University of Zagreb

Srecko Svaic
University of Zagreb

EXPERIMENTAL AND NUMERICAL STUDY OF THE FLOW AND HEAT TRANSFER IN PLATE HEAT EXCHANGER CHANNELS

Damir DOVIC[1], Srecko ŠVAIC[2]

University of Zagreb, Department of Thermodynamics, Thermal and Processing Technology, Zagreb, Croatia, Europe
Phone: +385 1 6168 510, Fax: +385 1 6156 940, [1]damir.dovic@fsb.hr, [2]srecko.svaic@fsb.hr

ABSTRACT

This paper presents an experimental and numerical study of the flow and heat transfer in corrugated chevron channels of plate heat exchangers. 3D CFD simulations were performed on two channel models, each consisting of 16 cells, with chevron angles b=28°and b=65° under laminar, transitional and fully turbulent flow conditions. Applied the RNG k-e and the RES models for turbulent flow simulation are presented and discussed. Computationally obtained flow patterns are analyzed and compared with recorded ones from the visualization tests. Different methods for evaluation of the simulated hydraulic and thermal characteristics are discussed and compared with experimental data from present measurements and literature.

1. INTRODUCTION

Plate heat exchangers (PHEs) are nowadays used in a wide range of applications for heating, cooling, evaporation and condensation purposes. Due to their low volume/surface ratio i.e. compactness, high overall heat transfer coefficient, low production and operational costs, they have found an increasing usage in place of conventional shell&tube heat exchangers. A number of investigations have been conducted with the aim of exploring the complex flow mechanisms that occur in a corrugated PHE channels. Also, several results fom the thermal-hydraulic tests have been reported revealing considerable disagreement between derived expressions for prediction of the heat transfer and pressure drop (Muley *et al*., 1999). A limited number of CFD studies on the flow through the smallest repeat unit of a channel (a single cell of a sinusoidal form, Figure 1) can be found in the literature (Ciofalo et al., 1996; Mehrabian, 2000). Those authors applied periodic flow conditions combined with imposed constant wall temperature and/or constant wall heat flux conditions. This work provides results from the 3D CFD analysis of the flow through 16 cells of two plate heat exchanger channels with different chevron angles: b=28° and b =65° (Figure 1). Such approach allowed for investigation of the flow characteristics and flow pattern formation starting from the channel entrance to the fully developed flow region. Additionally, avoiding a need for implementation of the periodic boundary conditions, as is case when the flow through only one cell is simulated, the heat transfer characteristics can also be presented in terms of the total heat flux exchanged between the central channel fluid and neighbor channel fluid under conditions that occur in a real heat exchanger, instead of determining only the heat transfer coefficient. The advantage of such approach is that it enables direct comparison of a computed with measured channel overall heat transfer capacity. Presented heat transfer and pressure drop characteristics are related to the fully developed flow conditions in the laminar, transient and turbulent region corresponding to the Re-numbers from Re=10 to Re=6000.

2. MODEL DETAILS

Three dimensional simulation of the PHE channel flow was performed using the computer code FLUENT. Similarly, like in a majority of computer codes within the field of the computational fluid dynamics, the finite volume method is employed here to convert the governing differential equations to algebraic equations suitable to be solved numerically. The computational domain consisting of 16 smallest repeat channel units (cells) is shown on Figure 1. Each cell (meshed using software package GAMBIT) is covered with 56160 hexahedral/wedge control volumes each consisting of 8/6 nodes placed on element edges, respectively, and distributed within each cell by means of the cooper meshing scheme. This ensured that all of cell cross sections perpendicular to the mean flow

direction are equally meshed. It was especially important to ensure that the fine grid in the near wall region (generated using a boundary layer option) is uniformly swept along the wall surface when initially created at cell flow inlet or outlet surface. The channel geometry (Figure 1) used in the simulation is consistent with the previously tested geometry, whereby the chevron angle was varied from b=28° to b=65° as the most influencing parameter on the flow, while the other parameters such as pressing depth b and corrugation width l (i.e. pitch p) were kept constant. Flow conditions considered here correspond to the following Re-numbers: Re=10, Re=700÷900 and Re=4600÷6000. This means that the present simulation should involve laminar, transitional and turbulent flow modeling. Fluids used in simulation were water at Re=(10÷6000) and aqueous solution of glycerol (85% of glyc. by weight) at Re=(10÷15) with identical properties to those of the test fluids used in the previously performed tests.

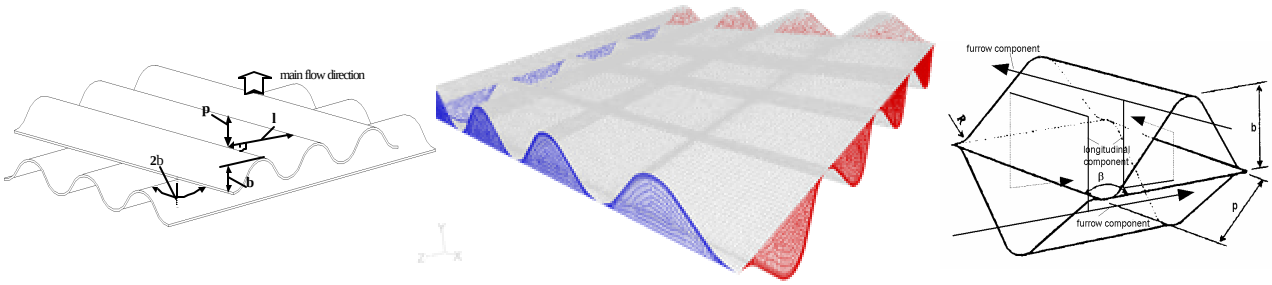

Figure 1: Geometry of a chevron channel composed of two corrugated plates together with the computational domain consisting of 16 cells and detail of a position of the flow components within particular cell

2.1 Governing equations and flow modeling

The standard set of equations discretized in order to solve laminar and turbulent flow comprises the equation for conservation of mass, conservation of momentum (Navier-Stokes equations) and conservation of energy. Written in the i-th direction for incompressible laminar flow with constant fluid properties and neglecting viscous dissipation terms they are given as

$$\frac{\partial u_j}{\partial x_j} = 0 \tag{1}$$

$$\frac{\partial u_i}{\partial t} + \frac{\partial (u_i u_j)}{\partial x_j} = -\frac{1}{r}\frac{\partial p}{\partial x_j} + n\frac{\partial^2 u_i}{\partial x_j^2} - \frac{1}{r} f_i \tag{2}$$

$$\frac{\partial T}{\partial t} + \frac{\partial u_j T}{\partial x_j} = a\left(\frac{\partial^2 T}{\partial x_j^2}\right) + \frac{1}{rc} S_T \tag{3}$$

where f_i is the body force per unit volume and S_T is the volumetric rate of heat generation.
A useful generalized representation of these equations is

$$\frac{\partial f}{\partial t} + \frac{\partial (u_j f)}{\partial x_j} = \Gamma \frac{\partial^2 f}{\partial x_j^2} + S \tag{4}$$

Here, the dependent variable f stands for a variety of quantities such as temperature, velocity component, turbulent kinetic energy etc, while S is the source term and G is the diffusion coefficient. The finite volume method employed here is based on integrating the conservation Equation (4) about each control volume within a computational domain. The face values of f are interpolated from the upstream cell center values using the second order upwind scheme.
In discretization of the momentum equation, the standard interpolation scheme was used to obtain the face values of pressure between centers of adjacent control volumes. For higher Re number flows (here at Re>4600) where additional swirling is expected, the PRESTO scheme was used instead (Patankar, 1980), since a large pressure gradients are expected between control volume centers. The SIMPLE pressure-velocity coupling algorithm was used to derive the equation for pressure from the discrete continuity equation. No benefits in terms of a faster

convergence have been observed when the SIMPLEC algorithm (Vandoormaal and Raithby, 1984) was used instead.

All calculations were performed in a double precision segregated steady state solver.

In the simulations of flows at Re>700 two different models were employed for turbulence modeling, namely the RNG k-e model and the Reynolds stress transport model (RES). In both approaches the Reynolds averaged equations need to be solved. Those equations can be written in the following form (incompressible flow with constant fluid properties):

$$\frac{\partial u_j}{\partial x_j} = 0 \tag{5}$$

$$r\frac{\partial u_i}{\partial t} + r\frac{\partial (u_i u_j)}{\partial x_j} = -\frac{\partial p}{\partial x_j} + m\frac{\partial}{\partial x_j}\left(\frac{\partial u_i}{\partial x_j} + \frac{\partial u_j}{\partial x_i}\right) - r\frac{\partial}{\partial x_j}\left(\overline{u_i' u_j'}\right) \tag{6}$$

Here, we can see that the additional terms appear, termed as the Reynolds stresses, in order to account for the effect of turbulence:

$$r\overline{u_i' u_j'} = m_t\left(\frac{\partial u_i}{\partial x_j} + \frac{\partial u_j}{\partial x_i}\right) - \frac{2}{3}\left(rk + \frac{\partial u_j}{\partial x_i}\right)d_{ij} \tag{7}$$

In order to close Equation (6) the Reynolds stresses which contain instantaneous values of velocity are modeled based on the Boussinesq hypothesis (Equation 7) in the k-e model, or in the RES model by means of solving the transport equations for each term of the Reynolds stress tensor together with one additional scale determining equation (normally for e). In the RNG k-e model two transport equations for k and e were solved (Equations (8)-(9)) while the turbulent viscosity m_t is computed as a function of k and e (Equation (10)):

$$r\frac{\partial k}{\partial t} + r\frac{\partial (u_j k)}{\partial x_j} = \frac{\partial}{\partial x_j}\left[\left(m + \frac{m_t}{s_k}\right)\frac{\partial k}{\partial x_j}\right] + G - re \tag{8}$$

$$r\frac{\partial e}{\partial t} + r\frac{\partial (u_j e)}{\partial x_j} = \frac{\partial}{\partial x_j}\left[\left(m + \frac{m_t}{s_e}\right)\frac{\partial e}{\partial x_j}\right] + C_1 G\frac{e}{k} - C_2 r\frac{e^2}{k} - R_e \tag{9}$$

where G represents the generation of turbulent kinetic energy due to the mean velocity gradients.

$$m_t = rC_m\frac{k^2}{e} \tag{10}$$

with C_m=0.0845, C_1=1.42, C_2=1.68.

In the standard k-e models turbulent Pr-numbers for k and e are taken as constants s_k=1.0 and s_e=1.3, respectively.

The RNG (renormalization group) based k-e model used in the present simulation has been proved to be more reliable and accurate for a wider class of flows than the standard k-e model. The main difference relative to the standard k-e model lies in the analytical derivation of the e transport equation.

Also, the RNG theory provides an analytical formula (more details in Choudhury, 1993) for turbulent Pr numbers s_k and s_e instead of using constant values, as well as the differential formula for the effective viscosity which accounts for low Re-number effects.

In the RES model the turbulent kinetic energy k needed for modeling a specific term in the transport equation for Reynolds stresses $r\overline{u_i' u_j'}$ is obtained directly from the normal Reynolds stress tensor $k = \frac{1}{2}\overline{u_i' u_i'}$.

Values of k near the wall are computed from the equation derived by contracting the exact transport equation for Reynolds stresses (Launder et al., 1975) which is essentially identical to Equation (8) used in the k-e model.

The dissipation tensor e_{ij} in the RES model is defined as

$$e_{ij} = \frac{2}{3}d_{ij}re \tag{11}$$

where the scalar dissipation rate e is obtained from the transport equation similar to the one from the k-e model (Equation (9)). The turbulent viscosity m_t is computed similarly to the k-e model (Equation (10)) taking C_m=0.09.

Convective turbulent heat transfer is modeled based on the Reynolds' analogy to turbulent momentum transfer where the modeled energy equation takes the following form for both the k-e and the RES model:

$$\frac{\partial T}{\partial t}+\frac{\partial u_j T}{\partial x_j}=\frac{1}{r}\frac{\partial}{\partial x_j}\left(\left(k+\frac{cm_t}{\Pr_t}\right)\frac{\partial T}{\partial x_j}\right)+\frac{1}{rc}S_T \tag{12}$$

In the standard k-e and RES model Pr_t=0.85 while in the RNG model Pr_t is calculated from the above mentioned analytical formula (Choudhury, 1993) as a function of m_{mol}/m_{eff} which is an advantage of the RNG model since it was experimentally confirmed that the turbulent Pr-numbers vary with the molecular Pr-number and turbulence (Kays, 1994).

In both described models the enhanced wall treatment was applied to resolve the viscosity affected region all the way down to the wall. The enhanced wall treatment combines two-layer modeling (viscosity affected region/fully turbulent region) with enhanced wall functions. The standard wall functions modeling would, instead, bridge this region between the wall and fully turbulent region. Such approach ensures accuracy when both coarse (wall function) meshes are used in high Re-number flows and also when fine low Re-number meshes are generated. The enhanced wall functions were derived by smoothly blending an enhanced turbulent wall law with the laminar wall law according to the following Equation (13) from Kader (1993) which gives a reasonable representation of the velocity profiles within the laminar sublayer, buffer region and fully turbulent outer region:

$$u^+ = e^{\Gamma}u^+_{lam}+e^{\frac{1}{\Gamma}}u^+_{turb} \tag{13}$$

In the two-layer modeling the domain is subdivided in two regions – fully turbulent and viscosity affected. In the fully turbulent region the k-e model and RES models are employed while in the viscosity affected region the one equation-model of Wolfstein (1969) is employed.

Two layer formulation of turbulent viscosity is smoothly blended with previously stated high Re-number definition for m_t from outer region (Equation (10)).

The similar procedure is used to ensure a smooth transition between algebraically specified e (Equation (14)) in the inner region and e obtained from the transport equation valid for outer region of turbulent boundary layer (Equation (9)).

$$e=\frac{k^{3/2}}{l_e} \tag{14}$$

Enhanced thermal wall functions are derived following the same approach used for the profile of u^+ (Equation (13)).

3.1 Boundary conditions

Inlet faces of the whole computational domain (Figure 1) were treated separately as the upper and lower corrugation velocity inlets while the opposite faces as flow outlets. At inlets of a particular channel half the velocity vector was aligned with the corresponding corrugation. This was supposed to be a good approximation of the actual flow condition at the channel entrance. The magnitude of the resultant velocity was determined from a measured volume flow rate and actual flow cross sectional area of the tested channel A_{cross}. The specification of the turbulent boundary conditions was the same for the k-e and the RES model i.e. in terms of the turbulence intensity ($I=u'/u_{avg}$= 1%) and turbulent viscosity ratio (m_t/m=10). The k and e values are then estimated from these quantities. In the RES model the Reynolds stresses at inlets are derived under the assumption of isotropy of turbulence ($\overline{u_i'u_j'}=0$, while the normal Re-stress component in each direction is obtained from $\overline{u_i'^2}=\frac{2}{3}k$). The outflow boundary conditions were applied at outlets of the simulated channel on which zero diffusion fluxes for all flow variables were imposed in the direction normal to the exit plane (Neumann boundary conditions). The zero diffusion flux condition applied at outflow faces means that the conditions of the outflow plane are extrapolated from within the domain and have no impact on the upstream flow, which is consistent with fully developed flow assumption. Thermal boundary conditions were defined in terms of the external heat transfer coefficient a_{ext} and external fluid temperature $T_{f,ext}$, known from the measurements. The heat flux to the wall is then computed as

$$q=a_{ext}\left(T_{f,ext}-T_{wall}\right) \tag{15}$$

4. RESULTS AND DISCUSSION

4.1 Flow pattern

Simulated flow distribution over the lower channel plate is shown on Figure 2 for different chevron angles and Re-numbers. The flow pattern recorded during the previously performed visualization tests (Dovic, 2000) is provided for comparison. At flow conditions corresponding to the mean channel Re-number Re=(10÷15) the criss-cross and wavy longitudinal flow pattern appear in the channels with b=28° and b=65°, respectively. The simulated and recorded flow patterns cannot be easily compared at higher Re-numbers due to the large mixing induced, that lead to the dispersion of the dye introduced in the channel flow core.

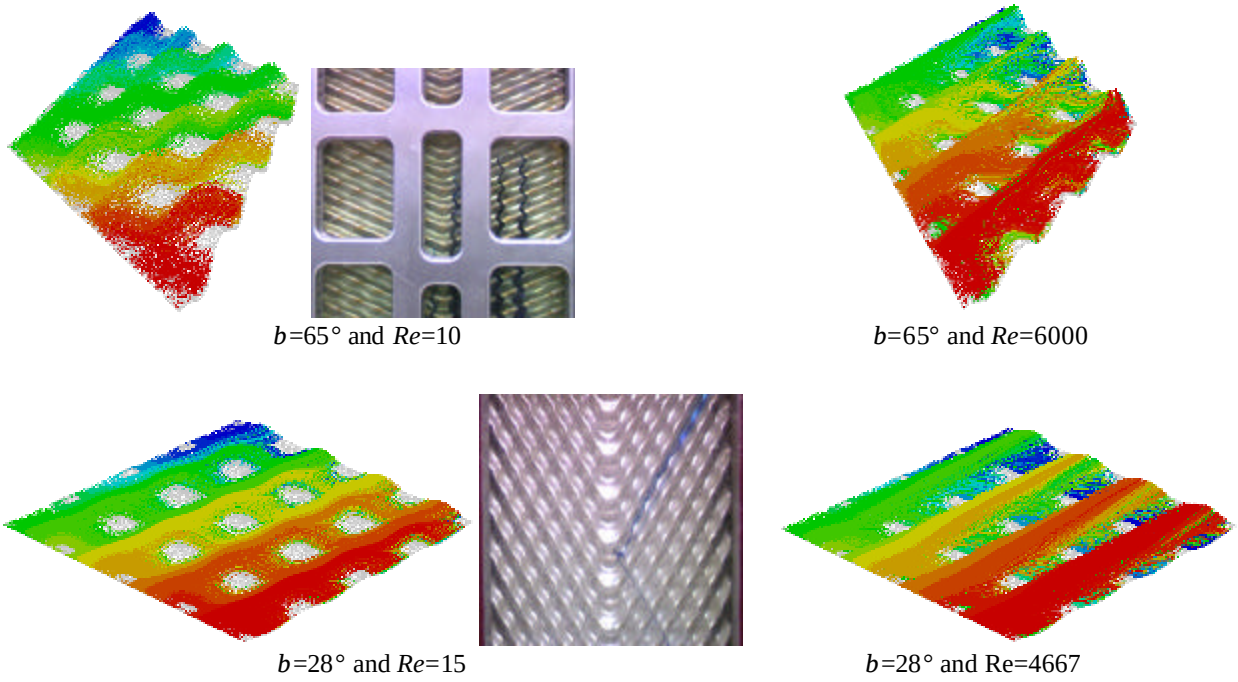

b=65° and Re=10 b=65° and Re=6000

b=28° and Re=15 b=28° and Re=4667

Figure 2: Simulated and experimentally recorded flow patterns in the channels with b=65° (wavy longitudinal pattern) and b=28° (criss-cross pattern) at low Re-numbers flow and fully turbulent high Re flow (Re>4667)

Simulated flow patterns confirm assumptions made in the previous works about existence of the two flow components, namely the furrow and the longitudinal one. The furrow component refers to the part of a fluid which does not change direction when passing throughout successive cells, while the longitudinal component changes direction within each cell flowing from one plate to the opposite one, as schematically shown on Figure 1.
Such a change of direction is believed to be accompanied by strong mixing within the cell, resulting in higher heat transfer coefficient as well as in higher pressure drop. An increase of the Re-number and aspect ratio b/l together with a decrease of the chevron angle b would promote the furrow component which results in the criss-cross (or furrow) flow pattern. The opposite conditions would promote the longitudinal component whose dominance is responsible for the wavy longitudinal flow pattern. It should be mentioned that the simulated turbulent flow field was shown to be qualitatively independent of the turbulence model employed in simulation.

4.2 Pressure drop

Figure 3 shows computed pressure drop of the simulated channels together with the measured data expressed in terms of the total pressure drop per unit of developed channel area and the Fanning friction factor f. The pressure drop is obtained as the difference between the total pressures (area weighted averages of node values) at cell inlets and outlets. Presented values for pressure drop comprise effects of the channel entrance parts where the shear is normally higher than in the part with fully developed flow conditions. The Fanning friction factor f is calculated using the expression

$$f = \frac{\Delta p}{4\left(\frac{L}{d_h}\right)\frac{r u_m^2}{2}} \tag{16}$$

and given in Figure 3 together with the measured data and experimental data from the literature (Muley et al., 1999). In the case of the channel with b=28° the characteristic length L is taken as the distance between the entrance and exit face along a single furrow provided that is the principal flow direction. In the case of the dominating longitudinal flow in the b=65° channel, L is defined as the shortest diagonal distance between two corners of simulated geometry. This way of defining a characteristic length with the respect to the main flow direction for particular channel could only ensure the Fanning friction factor to be comparable with measured values for the whole channel. In general, the simulated pressure drop (expressed in $\Delta p/m^2$) relatively slightly differ from the measured values at higher Re numbers (up to 10%, in average) while large discrepancies are present in the laminar flow at Re=(10÷15) when a highly viscous glycerol was set as a fluid. When comparison is made in terms of the Fanning friction factor f, then the differences between the simulated and measured results are higher at Re>700 and lower for laminar flow. This is believed to be a consequence of the present definitions of a characteristic length L and mean velocity u_m, which cannot completely reflect a rather complex flow distribution in the corrugated channel characterized by variable flow cross sections.

4.3 Heat transfer

As stated before, the heat transfer characteristics of the simulated channel are evaluated in terms of the total heat flux exchanged with the fluid flowing out of the channel (Figure 3). Heat flux reported refers to the single cell "far" from the channel entrances where the flow is proved to be both hydrodynamically and thermally fully developed (see Figure 2). The average heat flux for the whole simulated geometry is somewhat higher being affected by developing regions of more intensive heat (and momentum) transfer. Indeed, when comparing computed results with experimental ones, only the fully developed conditions are relevant figure of merit as they prevail in a real heat exchanger. The heat transfer coefficient could be evaluated based on the average channel flow heat flux, average wall temperature and averaged fluid temperature as defined by Equation (17). Such averaging, however, leads to the computational errors since the heat flux, wall temperature and corresponding mean fluid temperature can not be properly "coupled" in order to yield correct values for heat transfer coefficient at certain cross sections of the channel. In order to mitigate this affect to some extent, another approach of obtaining heat transfer coefficient based on the mean logarithmic temperature difference Δt_m is used instead, according to Equations (18)-(19). Such approach takes into account the change of the mean fluid temperature along the channel and yields (5-10)% better results, but still it can only include the mean values for a fluid temperature and wall heat flux, which finally results in a higher deviations from the measured values -up to 20 % (Figure 3) relative to the case when comparison is made in terms of the heat fluxes, when they go up to 10% (Figure 3). That is the main reason why simulations of the flow through one cell with periodical conditions cannot give a correct picture of the thermal characteristics as they do not allow use of the external convective heat transfer boundary conditions applied here, and therefore simulation of the exchanged heat. Simulated heat fluxes are (5÷15)% higher than the measured ones at the flow corresponding to Re>700 while deviations become again large for laminar flow, but they are less serious compared to the case with pressure drop calculations. The RES model gives better results for both simulated channels and all turbulent flow conditions (Re> 700) than the RNG k-e model. Thermal characteristics expressed in terms of $Nu/Pr^{1/3}$ are up to (10÷30)% higher than the measured ones at Re>700. In the laminar flow simulations the values of $Nu/Pr^{1/3}$ are close to the measured values only for channel with b=65° when water was set as a fluid instead of glycerol.

$$a_{16cells} = \frac{q_{av}}{\left(T_{wall,av} - T_{f,av}\right)} \tag{17}$$

$$\frac{1}{a_{16cells}} = \frac{1}{k} - \frac{1}{a_{ext}} \tag{18}$$

$$k = q_{devel.} / \Delta t_m = q_{devel.} / \frac{\left(t_{in} - t_{f,ext}\right) - \left(t_{out} - t_{f,ext}\right)}{\ln \frac{\left(t_{in} - t_{f,ext}\right)}{\left(t_{out} - t_{f,ext}\right)}} \tag{19}$$

$$Nu = \frac{a_{16cells} d_h}{l} \tag{20}$$

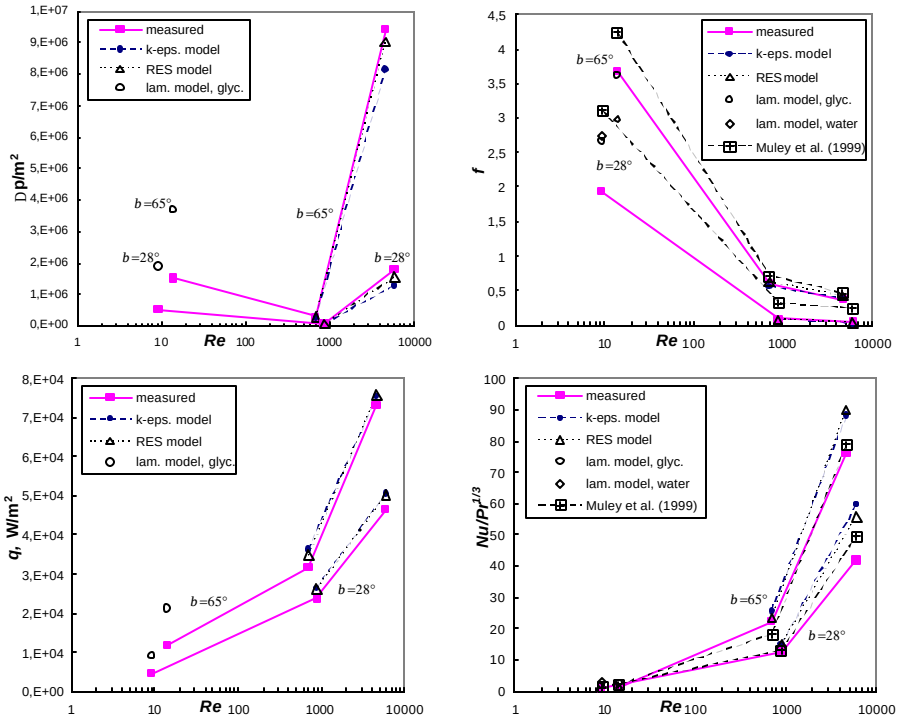

Figure 3: Simulated hydraulic and thermal characteristics of modeled channels with b=28° and b=65° compared to the experimental data from present measurements and literature (Muley *et al.*, 1999)

5. CONCLUSIONS

Numerical simulations of the flow distribution, momentum and heat transfer in corrugated chevron channels of plate heat exchangers were performed under laminar, transient and fully turbulent flow conditions on the model exchanger consisting of the 16 cells. The RNG k-e and RES models were used for turbulent flow simulations. Computed flow patterns compared with recorded ones confirm assumptions about occurrence of two flow components responsible for the criss-cross flow pattern in low angle channels (b<45°) dominated by the furrow component and for the wavy longitudinal flow pattern in high angle channels (b>45°) dominated by the longitudinal component. Higher velocities and deeper corrugations (higher aspect ratio b/l) would promote the furrow component which flows along particular furrow, while the longitudinal component, which changes direction in each cell, is promoted by opposite flow conditions and geometry. Comparison with performed thermal and hydraulic tests indicates that the pressure drop and heat transfer calculations give reliable results only for the transient and fully turbulent flows at Re>700, whereat the RES model was shown to yield more accurate results than the k-e model. In this case the simulated and measured results differ in average from 5% to 15 % when expressed in terms of the pressure drop per channel surface unit and exchanged heat flux. Larger deviations of the friction factor f from the measured values are attributed to the inappropriate definitions of the characteristic length and the mean velocity which do not fully reflect a complex flow distribution and variable channel geometry. The same deviations were observed in presentation of the thermal characteristics by means of $Nu/Pr^{1/3}$. This is believed to be a consequence of unavoidable averaging of the channel wall and fluid temperature in calculation of the heat transfer coefficient. For this reasons, computationally less expensive simulations performed on the single cell using a periodic boundary conditions are suspected to give a correct picture of the thermal characteristics, as they do not allow use of external heat transfer boundary conditions i.e. simulation of the heat flux exchanged between two fluids as a relevant figure of merit for comparison with experimental data.

NOMENCLATURE

A_{cross}	cross-sectional free flow area	(m^2)	**Subscripts**	
b	corrugation depth,	(m)	av	average

c	specific heat	(J $kg^{-1}K^{-1}$)	*devel.*	developed flow
d_h	hydraulic diameter, $2b/F$	(m)	*ext*	external
f	Fanning friction factor (Eq.)	(–)	*f*	fluid
k	turbulent kinetic energy	(m^2/s^2)	*i, j, k*	directions
L	characteristic channel length	(m)	*lam*	laminar
l_e	length scale	(m)	*m*	mean
Nu	Nusselt number	(–)	*t*	turbulent
p	pressure	(N/m^2)		
Pr	Prandtl number	(–)		
q	heat flux	(W/m^2)		
Re	Reynolds number, $u_{mean}d_h\rho/\mu$	(–)		
T	temperature	(K)		
t	time	(s)		
U	overall heat transfer coeff.	($Wm^{-2}K^{-1}$)		
u_i, u_j	velocity components	(m/s)		
a	heat transfer coefficient	($Wm^{-2}K^{-1}$)		
b	chevron angle	(°)		
$d_{i,j}$	Kronecker delta	(–)		
e	dissipation rate	(m^2/s^3)		
l	thermal conductivity	($W/m^{-1}K^{-1}$)		
r	density	(kg/m^3)		
m	dynamic viscosity	Pa s		

REFERENCES

Choudhury, D., 1993, Introduction to the Renormalization Group Method and Turbulence Modeling, *Fluent Inc. Technical Memorandum TM-107*.

Ciofalo, M., Stasiek, J., Collins, M.W., 1996, Investigation of Flow and Heat transfer in Corrugated Passages-II. Numerical simulations, *Int. J. Heat Mass Transfer*, vol. 7, no. 1: p. 165-192.

Dovic, D., 2000, The Analysis of Single-Phase Flow in Chevron Channels of Plate Heat Exchangers, *Int. MSc Thesis*, Energy Department, Royal Institute of Technology, Stockholm, Sweden.

Kader, B., 1993, Temperature and Concentration Profiles in Fully Turbulent Boundary Layers, *Int. J. Heat Mass Transfer*, vol. 24, no. 9: p. 1541-1544.

Kays, W. M., 1994, Turbulent Prandtl Number - Where Are We? *J. Heat Transfer*, vol. 116, p. 284-295.

Patankar, S.V., 1980, *Numerical Heat Transfer and Fluid Flow*, Hemisphere, Washington, D.C., p. 176.

Launder, B. E., Reece, G. J., Rodi, W., April 1975, Progress in the Development of a Reynolds-Stress Turbulence Closure, *J. Fluid Mech.*, vol. 68, no. 3: p. 537-566.

Mehrabian, M.A., Poulter, R., 2000, Hydrodynamics and Thermal Characteristics of Corrugated Channels: Computational Approach, Appl. Mathematical Modeling, v. 24, p. 343-364.

Muley, A., Manglik, R.M., Feb. 1999, Experimental Study of Turbulent Flow Heat Transfer and Pressure Drop in a Plate Heat Exchanger With Chevron Plates, *J. Heat Transfer, Transactions of the ASME*, vol. 121, p. 110-117.

Vandoormaal, J. P., Raithby, G. D., 1984, Enhancements of the SIMPLE Method for Predicting Incompressible Fluid Flows, *Numer. Heat Transfer*, vol. 7, p. 147-163.

Wolfstein, M., 1969, The Velocity and Temperature Distribution of One-Dimensional Flow with Turbulence Augmentation and Pressure Gradient, *Int. J. Heat Mass Transfer*, vol. 12, p. 301-318.